Comparison between Standard and Modified Forward Scattering Spectrometer Probes during the Small Cumulus Microphysics Study

FRÉDÉRIC BURNET AND JEAN-LOUIS BRENGUIER

CNRM/GAME, Météo-France/CNRS, Toulouse, France

ABSTRACT

Microphysical measurements performed during the Small Cumulus Microphysics Study (SCMS) experiment are analyzed in order to examine the instrumental limitations of forward scattering spectrometer probes (FSSPs). Complementary information collected with a modified version of the instrument, the Fast-FSSP, are used to address crucial issues such as the size calibration of the spectrometers and the effects on the measured spectra (distortion and broadening), of beam inhomogeneities, of variations of the sampling section, and of the coincidence of particles. Their impact on the calculation of liquid water content is evaluated by the comparison with measurements performed with a hot-wire probe and a particle volume monitor. In addition to the statistical approach that aims at evaluating the typical uncertainty of the measurements, special attention is given to the identification of circumstances under which some of the instrumental limitations combined are likely to affect significantly the accuracy of the measurements. The overall data quality is illustrated in the data summary of the 10 missions flown with the Météo-France Merlin-IV during SCMS. Droplet concentration measurements performed with the standard and the Fast-FSSP, and statistically processed for each flight separately, agree to within a bias lower than 10% and a standard deviation of $\pm 20\%$. The derived liquid water content measurements, compared to the hot-wire probe, exhibit a larger standard deviation of $\pm 30\%$, with a substantial degradation at high droplet concentration due to droplet spectra distortion by droplet coincidences in the detection beam.

1. Introduction

The Small Cumulus Microphysics Study (SCMS), focused on the onset of precipitation in cumulus clouds, took place in July and August 1995 in the Cape Kennedy area (Florida). Three instrumented aircraft were involved, the University of Wyoming (UWYO) King-Air, the National Center for Atmospheric Research (NCAR)[1] C130, and the Météo-France Centre d'Aviation Météorologique (CAM)[2] Merlin-IV. An extensive microphysical dataset was collected during the field experiment with Commonwealth Scientific and Industrial Research Organisation (CSIRO) hot wires (King et al. 1978), a particle volume monitor, PVM-100A (Gerber et al. 1994), a cloud drop spectrometer (CDS) (Lawson and Cormack 1995), forward scattering spectrometer probes, FSSP-100[3] and the Fast-FSSP (Brenguier et al. 1998), a modified version of the FSSP-100.

Droplet spectra measurements with FSSPs are affected by diverse sources of uncertainty that have already been identified and extensively discussed (Dye and Baumgardner 1984; Baumgardner et al. 1985; Cooper 1988; Brenguier 1989; Baumgardner and Spowart 1990). They are related to the nonuniformity of light intensity in the laser beam, to variations of the size calibration and of the sampling section of the instrument, and to the effects of coincidence in the sampling volume. The measured droplet spectra are not all similarly affected by these instrumental limitations. For example, variations of the sampling section are more significant for small droplets with a diameter close to the detection limit of the instrument; coincidence effects are more severe at high cloud droplet number concentration (CDNC). It is not straightforward in fact to evaluate the accuracy of the measurements when these effects are combined, when measuring a high concentration of small droplets for example. Numerical models of probe functioning have been developed for simulating these combined effects. Cooper (1988) followed a probabilistic approach with the transfer matrix of the instrument that indicates the probability for a droplet, ideally counted in one size class, to be counted in an another one (spectral broadening). The model was also extended to the coincidence of two particles (Cooper 1988). The inversion of the transfer matrix system allows retrieval of the actual droplet spectrum from the measured one. High-level coincidence of three or more droplets has also been simulated with a stochastic, or Monte Carlo, version of the model (Perrin et al. 1998), but there is presently no operational technique for inversion of that

---

stochastic model. The difficulty to reproduce in the laboratory the same conditions as in flight is a serious obstacle to the experimental analysis of the probe response to droplets of different sizes, which is required for validation of the model of probe functioning.

The analysis of the extensive SCMS dataset presented here offers an alternative to the laboratory experiments. The droplet spectra that were collected are unknown, but one can expect that the different instruments converge in average to the actual response. In addition, since measurements were collected in cumulus clouds, one can use the adiabatic prediction as an absolute upper limit of the measured liquid water content (LWC).

The objectives of this study are threefold. First, the analysis aims at providing an evaluation of the data quality with quantification of the variability in the measurements of CDNC, mean volume diameter (MVD), and LWC for the whole SCMS campaign. Second, the diversity of the dataset is used to focus on specific samples, depending on the droplet sizes or the CDNC value, in order to examine separately the diverse sources of uncertainty. Finally, variations of some key parameters are documented for validation of the model of probe functioning.

The SCMS dataset is particularly suited to these objectives with numerous flights, a large diversity of microphysical conditions, and four FSSP probes: three standard versions with different electronic settings and size calibrations, and the Fast-FSSP. The finer size resolution of the Fast-FSSP, and its additional parameters, pulse duration and interarrival time, are particularly useful for the interpretation of the standard probes functioning. The list of flights and instruments considered in this study are indicated in Table 1. Comparisons are made between the Fast-FSSP, FSSP-100, CSIRO, and PVM-100A data, with statistics over the whole campaign, and for each flight separately. The microphysical data are then summarized for the 10 missions flown by the Merlin-IV during SCMS to illustrate the overall accuracy of the campaign.

2. Description of the FSSP-100 and Fast-FSSP

Very detailed descriptions of the FSSP-100 are already available in the literature (Dye and Baumgardner 1984; Baumgardner et al. 1985; Brenguier 1989). The Fast-FSSP is a modified version of the FSSP-100 with new electronics that measure for each detection, the pulse amplitude with 255 size classes instead of 15 in the standard probe, pulse duration and interarrival time from the previous detection with a resolution of 1/16 μs, and a parameter relative to the location where the detected particle crosses the beam (Brenguier et al. 1998). A few typical features of the FSSPs that are important for the following discussions are summarized here.

The FSSP sampling tube, parallel to the airflow, has an internal circular cross section of 40 mm in diameter.

TABLE 1. Summary of the analyzed dataset; "hc" refers to the NCAR *C-130* and "me" refers to the CAM *Merlin-IV*.

Date	Flight	UWYO-FSSP	NCAR-FSSP	CAM-FSSP	FAST-FSSP	CSIRO	PVM-100A
22 Jul	hc9504		Yes		Yes		Yes
24 Jul	hc9505		Yes		Yes		Yes
26 Jul	hc9506		Yes				Yes
28 Jul	hc9508		Yes				Yes
31 Jul	hc9510		Yes				Yes
4 Aug	hc9511		Yes				Yes
	me9505			Yes	Yes	Yes	
5 Aug	hc9512		Yes				Yes
	me9506			Yes	Yes	Yes	
6 Aug	hc9513		Yes				Yes
	me9507			Yes	Yes	Yes	
7 Aug	hc9514		Yes				Yes
	me9508			Yes	Yes	Yes	
8 Aug	hc9515		Yes				Yes
	me9509			Yes	Yes	Yes	
9 Aug	me9510			Yes	Yes	Yes	
10 Aug	hc9516		Yes				Yes
	me9511			Yes	Yes	Yes	
11 Aug	hc9517		Yes				Yes
	me9512			Yes	Yes	Yes	
12 Aug	hc9518		Yes				Yes
	me9513			Yes	Yes	Yes	
	me9514	Yes	Yes	Yes	Yes	Yes	
13 Aug	hc9519		Yes				Yes
	hc9520		Yes				Yes

It is traversed, perpendicular to the airflow, by a laser beam focused to a diameter of about 0.2 mm at the tube axis. This incident beam is then masked by a dump spot in front of the detection optics. Droplets crossing the beam are detected by measuring the intensity of light scattered forward around the dump spot. Due to the optical setting of the instrument, droplets are, however, detectable only when they cross the incident beam within about 7.5 mm of the focal point. The corresponding cross section of the beam, perpendicular to the airflow, is referred to as the total *sensitive* area S_T (15 × 0.2 mm^2 = 3 mm^2). The beam intensity is not uniform for all particle intersections of this area, and droplets of the same size can be counted in different size classes, hence producing spectrum broadening. It is therefore more accurate to select for sizing only those droplets that cross the beam through a narrower central section, hereafter referred to as the *efficient* sampling section (S_{EFF}), where the incident light intensity is more uniform, and where the collected angles of scattering are similar. Beam intensity mapping (Baumgardner and Spowart 1990) shows a cylindrical symmetry, with a bell-shaped profile of light intensity across the beam. On both sides of the focal plane, the beam intensity also decreases along the beam axis because of the beam divergence. It follows that a particle receives the maximum incident light when it crosses the axis plane, perpendicular to the airflow. This occurrence also corresponds to the peak amplitude of the detected pulse that is recorded by the acquisition system. The objective for accurate sizing is thus to select an area centered at the focal point, limited along the

a) Exemples of droplet trajectories
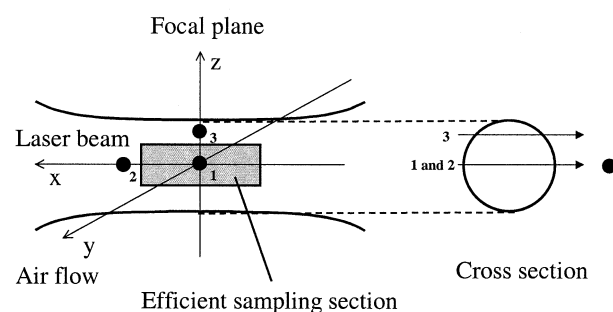
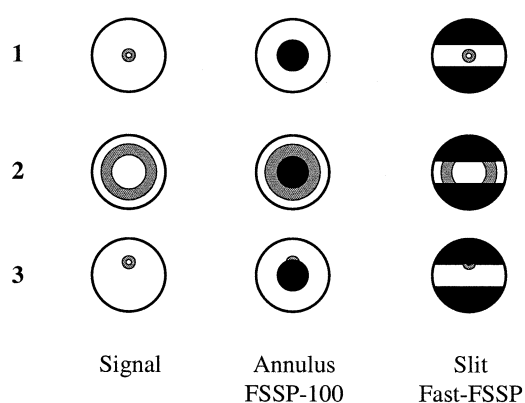**b) Corresponding scattering images on the diodes**

FIG. 1. Schematic of the efficient sampling section selection: (a) examples of droplet trajectories across the laser beam (longitudinal and cross section) and (b) corresponding scattering images on the detection diodes.

beam axis to the nondivergent section of the beam (about 3 mm), and close to its axis (within 50%–60% of the beam diameter).

In the FSSP-100 this selection involves two steps. The first one is based on optical principle, using two detection diodes. The scattered light is split in two directions. One diode collects the signal for sizing. It is referred to as the *signal* diode. The second one, referred to as the *annulus* diode, is used for the selection. It is covered at its center by a small mask so that the image of a droplet crossing at the beam focal plane (1 and 3 in Fig. 1a) is projected on the mask and the diode receives less scattered light. On the contrary, the scattering image of particles crossing far from the focal plane (2 in Fig. 1a) is broader, so that scattered light passes around the mask. The comparison between signal and annulus amplitudes thus allows the rejection of particles crossing the beam too far from the focal plane. The selected area is referred to as the depth of field (DOF) cross section S_{DOF}. The droplet counted rate used for CDNC calculation is the number of particles counted per second in DOF. However, droplet sizing requires a

second step in order to reject some of the DOF accepted droplets, that is, those crossing the beam edge where the beam intensity is lower. This is performed by comparing the pulse duration to its running mean value. Droplets crossing the beam edge (3 in Fig. 1a), which is a shorter chord thought the beam, exhibit short pulse durations and they are rejected for sizing. This step is referred to as the *pulse duration* selection. The FSSP-100 acquisition system only records the droplet size information for detections that have been selected for DOF and pulse duration.

In the Fast-FSSP, both steps are accomplished with a slightly different optical principle. The second diode is entirely covered by a mask except for a narrow slit at the center that is oriented parallel to the airflow. A particle crossing out of the focal plane produces a broad image that is partially masked by the slit (2 in Fig. 1b). When the particle crosses at the focal plane, close to the beam edge, it produces a narrow image on the side of the slit (3 in Fig. 1b). Only droplets close to the beam axis and within a short distance of the focal point (1 in Fig. 1b) produce images centered on and smaller than the slit. This setting, originally developed for the FSSP-300 (Baumgardner et al. 1992), thus combines DOF and pulse duration selections. The corresponding droplet rate is used for CDNC and spectral shape calculations.

Consequently, the FSSP-100 and Fast-FSSP sampling sections for CDNC or spectral shape calculations are not identical. In the FSSP-100 the DOF selection ratio $R_{DOF} = S_{DOF}/S_T$ is about 20%. The spectral shape is derived from only DOF counts that are also selected for their pulse duration (a selection ratio of about 50%) that is overall $R_{EFF} = S_{EFF}/S_T = 10\%$ of the total counts.

In the Fast-FSSP, CDNC, and spectral shape are derived from the same set of selected counts. The efficient area depends upon the settings of the detection amplifiers. During SCMS it was set to $S_{EFF} = 0.13$ mm^2 (see Fig. 4 in Brenguier et al. 1998); that is, $R_{EFF} = 4.5\%$. The Fast-FSSP acquisition system, in contrast to the standard system, records the four parameters: pulse amplitude, duration, interarrival time, and position flag for each detection individually.

3. Measurements of the droplet size distribution and probe limitations

The droplet size distribution is characterized by the continuous function $f(r)dr$ that represents the droplet number concentration density (cm^{-3} μm^{-1}) at the droplet radius r. Airborne spectrometers proceed by droplet counting in discrete size classes and thus provide an approximation of the size distribution with the droplet spectrum or mean droplet concentration density C_i per size class i:

$$C_i = \lambda_i/(S_i v_a \Delta \phi_i), \qquad (1)$$

where i refers to the class of droplets with a diameter between ϕ_i and ϕ_{i+1}, λ_i is the droplet counted rate, S_i

TABLE 2. Calibration scales of the FSSP-100 and the Fast-FSSP. The diameter value (μm) in each line represents the lower boundary of the indicated size class. For the Fast-FSSP, only 15 classes are indicated, with the corresponding class number, for the first flight of the campaign on the NCAR C-130 (hc9504) and for the last one on the Merlin-IV (me9514). The last line contains the upper boundary of the probe's diameter range.

FSSP-100				Fast-FSSP		
Class no.	UWYO	NCAR	CAM	Class no.	hc9504	me9514
1	3.5	2.6	2.7	8	4.64	5.57
2	6.5	5.2	6.2	15	6.78	8.28
3	9.5	9.8	9.7	20	8.18	10.05
4	12.5	13.2	13.2	30	10.71	13.24
5	15.5	16.4	16.6	40	12.91	16.00
6	18.5	18.5	20.1	50	14.84	18.41
7	21.5	22.1	23.6	60	16.54	20.52
8	24.5	26.9	27.0	70	18.05	22.39
9	27.5	30.6	30.5	80	19.41	24.07
10	30.5	33.0	34.0	100	21.81	27.03
11	33.5	39.4	37.4	125	24.49	30.33
12	36.5	42.0	40.9	150	27.06	34.50
13	39.5	47.6	44.4	175	29.63	36.69
14	42.5	48.9	47.9	200	32.16	39.82
15	45.5	49.1	51.3	225	34.43	42.60
Upper boundary	48.5	52.0	54.8	255	36.29	44.74

is the sampling cross section, v_a is the particle speed through the sampling section, and $\Delta\phi_i$ is the class width.

In the FSSP-100 the droplet size information is only available for detections that have been selected for DOF and pulse duration. Because the corresponding sampling section is more difficult to measure than the DOF sampling section S_{DOF}, it is common to proceed in two steps. First, the spectral shape is calculated based on those selected counts, assuming a constant value for S_i. Second, the total droplet concentration is derived from the DOF selected counts λ_{DOF}, as $N = \lambda_{DOF}/(S_{DOF}v_a)$. The droplet spectrum is finally obtained by scaling the previously derived histogram by this total droplet concentration ($\Sigma \ C_i = N$). Therefore, it is common with the FSSP-100 to distinguish between spectral shape (first step) and CDNC (second step) calculations. In particular, problems related to the pulse duration selection only affect the spectral shape calculation. With the Fast-FSSP both steps are combined using S_{EFF} instead of S_{DOF}.

In fact each of the parameters in (1) contributes to the uncertainty in the measurement of a droplet spectrum, and the main difficulty is to assess their respective contributions.

- The precise definition of the size class boundaries, ϕ_i and ϕ_{i+1}, is referred to as the size calibration of the probe that relates the measured pulse amplitude to a scale of droplet diameters (Table 2). It is derived from Mie calculations of the forward scattered light integrated over the solid angle collected by the FSSP optics. The adequacy of the standard calibration function is discussed in Dye and Baumgardner (1984). In practice the probes shall be regularly calibrated using glass beads to account for possible variations of the optical alignment and dust contamination of the lenses. An interesting self-calibration technique has been developed for the Fast-FSSP. Because the relationship between droplet diameter and measured scattered light intensity is not monotonic, some values of intensity have a higher probability to be measured. They are precisely related to specific values of droplet diameter. The identification in the dataset of such frequently measured values provides for each flight the calibration coefficients of the instrument (Brenguier et al. 1998).

- Despite the DOF and pulse duration selection procedures, the incident light intensity is not perfectly uniform throughout the efficient sampling section, and droplets of the same diameter can still be counted in different size classes depending on where they cross the beam. If the nominal or expected size is defined as the value that is measured when a droplet crosses the beam center, where the light intensity is maximum, such a missizing due to beam inhomogeneities results in spectrum broadening toward smaller sizes than expected (Baumgardner and Spowart 1990). In practice, the size calibration is performed by spreading glass beads randomly through the detection beam providing an intermediate diameter reference, with broadening occurring on both sides of the reference.

- The probe sampling section S_i is currently defined as a constant for data processing, though laboratory studies suggest that it could be slightly dependent upon the droplet diameter (Dye and Baumgardner 1984). This effect results in a spectrum distortion and errors in CDNC.

- The counted rate is lower than the actual rate because of coincidence losses, when two, or more, droplets cross the beam simultaneously. The actual rate can be derived from the counted one using statistical formulas and either the counted rate, the probe activity (sum of pulse durations and electronic delays), a combination of both (Brenguier 1989), or the measured frequency distribution of interarrival times between detections (Baumgardner 1986). A pulse amplitude of coincident droplets is generally higher than the ones the droplets would produce separately. Therefore, a coincidence event reduces the counted rate in the size classes of the coincident droplets and increases the counted rate in a larger size class. Coincidences are thus a source of spectrum broadening toward larger sizes than expected (Perrin et al. 1998).

- Airflow simulations have shown that the particle speed through the FSSP sampling tube is lower than the aircraft speed as it is measured with the onboard reference system (Norment 1988). Depending on how the airflow is slowed down in the vicinity of the probe and within its sampling tube, as well as the possibility of inertial separation of droplets of different sizes in the airflow, this effect can result in spectral distortion and CDNC errors. It will not be discussed here be-

cause it affects similarly the four FSSPs that are compared in this paper.

The ideal procedure for characterizing the probe's limitations would be in the laboratory to spread droplets of same sizes in various locations of the detection beam. However, the generation of small droplets and their trajectory control is a challenge, especially at a velocity comparable to the current aircraft velocity. For example, the droplet generator described by Wendisch et al. (1996) produces droplets bigger than 15 μm at a speed slightly larger than 1 m s^{-1}. An alternative approach is considered here, which consists in analyzing a large dataset with very different microphysical characteristics in order to address the various issues separately.

a. Size calibration and beam inhomogeneities

The last Merlin-IV SCMS flight (me9514) was devoted to FSSP intercalibration. The three FSSP-100 and the Fast-FSSP were all mounted on the fuselage nose pods so that they were separated by less than 2 m, hence allowing close comparison of the measurements.

Figure 2 shows three examples of droplet spectra sampled in a cumulus cloud at various altitudes: 980, 660, and 1250 m for Figs. 2a,b,c, respectively (the cloud base was at about 450 m). The main difference between the three FSSP-100s is in the first size class, where the CAM shows a greater density than the NCAR and UWYO instruments. In fact only the CAM-FSSP was operated with the *delay mode* for pulse duration selection (Dye and Baumgardner 1984), an option that is known for increasing the counts in the first size class. The delay mode consists in measuring pulse duration at midamplitude instead of measuring it at a fixed threshold value. It is recommended by PMS to correct for a possible underestimation of the concentration density of the smallest droplets. However, in Fig. 2c the four instruments agree in showing a spectrum of large droplets, with a very low concentration density at diameters smaller than 10 μm. It is unlikely that the actual concentration density specifically increases in the first FSSP size class, as in the CAM-FSSP spectrum, while it is so low in the second class. Moreover, the CAM-FSSP spectra show a systematically high concentration density in the first size class, even in spectra of very large droplets at the upper limit of the diameter range, with a very low concentration density in the intermediate classes. It is thus concluded that the delay mode overestimates the number density in the first CAM-FSSP size class. The comparison with the Fast-FSSP even suggests that FSSP-100 measurements in the *normal mode* (NCAR- and UWYO-FSSPs) also overestimate the concentration density of the smallest droplets. Such an assessment though cannot be generalized to all FSSP probes because the response of this instrument to small droplets in the first class is very sensitive to the setting of the noise bias offsets in the detection module.
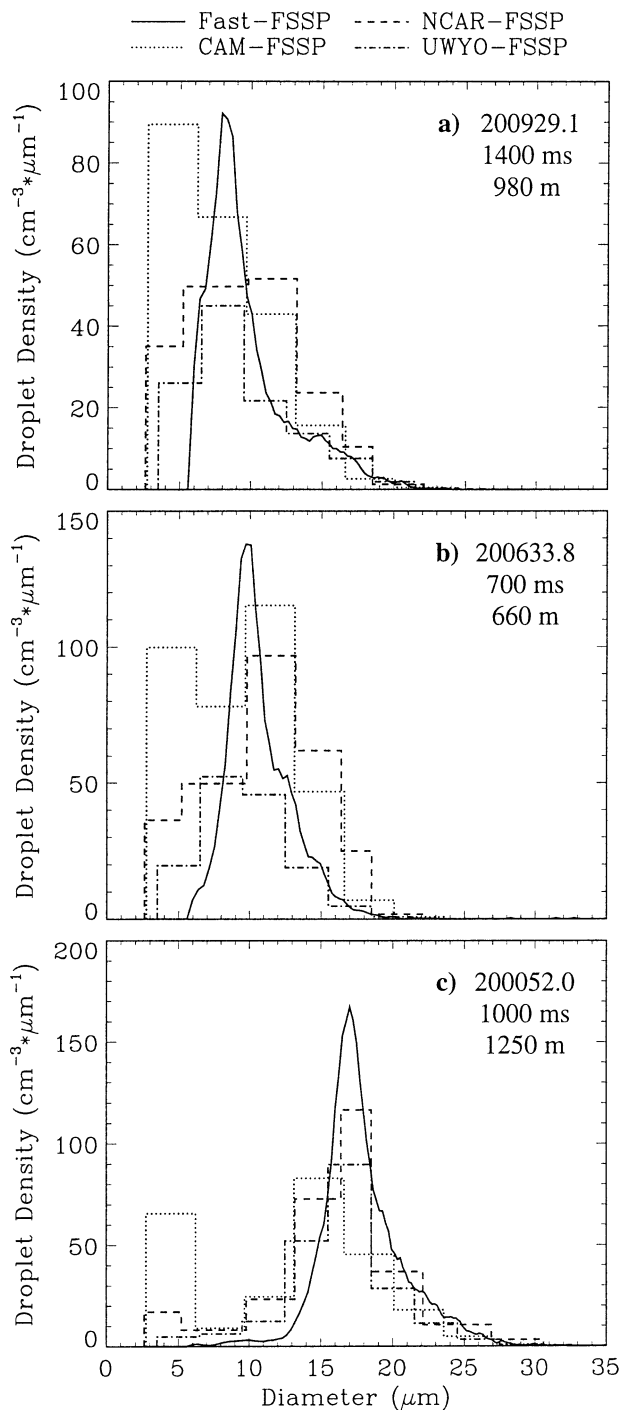

FIG. 2. Droplet spectra measured with the Fast-FSSP and the three FSSP-100s during the Merlin-IV intercalibration flight me9514. Sampling time (UTC), sample duration (ms), and sampling altitude (m), as indicated in the legend.

The droplet spectral width is a crucial parameter for the study of droplet condensational growth and the onset of precipitation (Brenguier and Chaumat 2001; Chaumat and Brenguier 2001). Specifically, a significant proportion of droplets much smaller than the mode is a feature

TABLE 3. Spectral characteristics of the three examples shown in Fig. 2. The spectral width is derived as the spectrum std dev.

	FFSSP	CAM	NCAR	UWYO
Lower size limit* (μm)	5.6	6.2	5.2	6.5
(a) Mean diam (μm)	9.9	10.2	10.5	10.7
Mean vol diam (μm)	10.9	11.3	11.8	11.9
Mode (μm)	8.5	9.3	10.5	9.0
Spectral width (μm)	3.08	2.82	3.21	3.33
(b) Mean diam (μm)	10.9	11.2	11.6	10.5
Mean vol diam (μm)	11.4	12.1	12.7	11.4
Mode (μm)	10.0	11.0	11.5	9.4
Spectral width (μm)	2.37	2.80	3.20	2.66
(c) Mean diam (μm)	18.0	16.0	16.8	16.5
Mean vol diam (μm)	18.5	17.0	17.9	17.4
Mode (μm)	16.8	15.4	17.1	16.6
Spectral width (μm)	2.95	3.79	4.06	3.42

* Without FSSP-100 first class.

that has often been reported in the literature (Hill and Choularton 1985; Bower and Choularton 1988). Many attempts have been made to explain the presence of small droplets by partial evaporation following entrainment-mixing processes, combined with secondary activation of entrained cloud condensation nuclei. However, it is still not yet clear how much of this feature is due to instrumental spectrum broadening. The three examples shown in Fig. 2 are among the narrowest droplet spectra sampled during the flight. Due to the size dispersion effect of the instrument the measured spectrum probably cannot be narrower than the actual one, and it can be surmised that the actual spectra are at least as narrow as measured with the Fast-FSSP. The difference in spectral broadening between the two instruments is attributed partly to the finer size resolution of the Fast-FSSP and partly to the larger efficient section of the FSSP-100 (0.3 mm^2) compared to the Fast-FSSP one (0.13 mm^2).

Because the detection threshold of the Fast-FSSP was set to 5.6 μm, a value close to the upper limit of the first FSSP-100 size class (Table 2), the FSSP-100 data are now processed without the first size class. Table 3 summarizes characteristic values of the three spectra shown in Fig. 2, with the mean and mean volume diameters, the spectral mode, and the spectral width, calculated as the standard deviation in diameter. The differences in diameters are of the order of 1 μm, but these differences can be as large as 2 μm, for example, between the Fast-FSSP and the CAM-FSSP mean diameters in the third example. For the spectral width, most of the differences are lower than 0.5 μm, with the exception of the Fast-FSSP versus NCAR-FSSP in the second example, and the Fast-FSSP versus the CAM and NCAR-FSSPs in the third example. It can also be noticed that the spectral width measured with FSSP-100 probes is usually larger than that of the Fast-FSSP, a feature that reflects the finer size resolution of the Fast-FSSP, with 255 size classes instead of 15 in the standard

instrument, and the efficiency of the *slit* versus pulse duration selection procedure.

Most of the spectra sampled during SCMS were in fact broader than the examples presented in Fig. 2. In order to generalize the above analysis, MVD values of the 10-Hz sample measured by the four instruments are thus compared in Fig. 3. Figure 3a, for the Fast-FSSP versus CAM-FSSP, includes data from the 10 SCMS flights of the Merlin-IV from me9505 to me9514 (41 957 samples). Figure 3b, for the Fast-FSSP versus the NCAR-FSSP, includes data from two flights of the NCAR C-130, hc9504 and hc9505, and from the intercalibration Merlin-IV flight, me9514 (8454 samples). Finally Fig. 3c, for the Fast-FSSP versus the UWYO-FSSP, is limited to the Merlin-IV intercalibration flight (1614 samples).

The nonlinear size calibration scale of the Fast-FSSP is derived from modeling of Mie scattering and scattered light collection by the Fast-FSSP optics. The calibration coefficients were calculated for each flight, with the self-calibration technique described in Brenguier et al. (1998). The nonlinear calibration of the NCAR-FSSP follows the procedure described in Dye and Baumgardner (1984). The size scales of the UWYO- and CAM-FSSPs are linear (the class width $\Delta\phi_i$ is constant), as recommended by PMS, with the standard scale for the UWYO instrument, while the size offset and class width of the CAM-FSSP were adjusted by intercalibration with the Fast-FSSP (Table 2).

Despite the fact that the CAM-FSSP was calibrated versus the Fast-FSSP, Fig. 3a reveals that there are still noticeable discrepancies between the two instruments. Fast-FSSP MVD values are underestimated with respect to the values measured by the CAM-FSSP in the range from 8 to 11 μm, and they are overestimated in the range from 12 to 18 μm. The two instruments only agree for MVD values larger than 20 μm. The same feature is observed in Fig. 3c for the comparison of the Fast-FSSP with the UWYO-FSSP measurements. In Fig. 3b, for the Fast-FSSP versus NCAR-FSSP the default of linearity is less pronounced, hence suggesting that the nonlinear scale recommended by Dye and Baumgardner (1984) is more suited than the linear one. These observations indicate that the choice of the calibration scale for processing FSSP data has a significant impact on measurements of spectral characteristics such as MVD, particularly in the small diameter range where the Mie calibration curve of the instrument is not monotonic. The above analysis reveals that the accuracy of FSSP MVD measurements in the range from 5 to 30 μm is of the order of ± 1 μm in standard deviation, and that the standard linear calibration scale introduces an additional positive or negative bias of the same order, depending on the size range. For example, a 1-μm error in MVD at 15 μm leads to an error of 20% in the derived LWC.
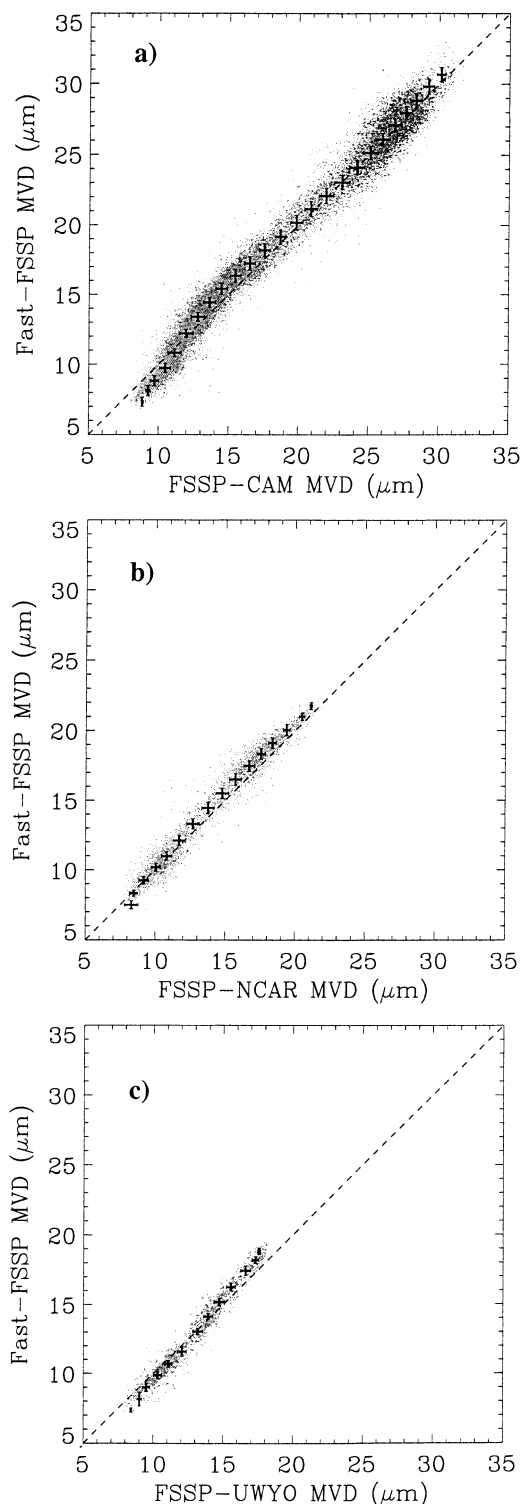
FIG. 3. Scatterplots of the 10-Hz sample mean volume diameter values measured with the Fast-FSSP vs the values measured with (a) the CAM-FSSP (from the 10 Merlin-IV flights me9505 to me9514), (b) the NCAR-FSSP (from two NCAR C-130 flights hc9504 and hc9505, and the Merlin-IV intercalibration flight me9514), and (c) the UWYO-FSSP (from the Merlin-IV intercalibration flight me9514). Mean value and std dev are indicated for every 1-μm-diameter step.

b. Variations of the sampling section

In using (1) for CDNC calculations it is always assumed that the sampling section S_i does not depend upon droplet size. However, measurements in the laboratory (Dye and Baumgardner 1984) revealed that the DOF increases with decreasing droplet sizes. This feature can be documented with the SCMS dataset by analyzing the ratio of selected to total counts that is equivalent to the DOF acceptance ratio $R_{DOF} = S_{DOF}/S_T$, though the difficulty then is to determine if changes in R_{DOF} with droplet size are due to S_{DOF} or S_T variations. Big droplets are producing a detectable pulse throughout the whole sensitive area that is thus constant and only limited by the optical probe setting. Small droplets in contrast are not detected over the whole sensitive area because of the decrease of the incident light intensity far from the focal point. The size detection limit of the instrument is not sharply defined. One should rather consider a detection range from ϕ_1 to ϕ_2; ϕ_1 is the diameter of a droplet producing a detectable pulse only when it crosses the beam at the center, where the light intensity is maximum. Its sampling section, limited to a point, is null. Here, ϕ_2 is the diameter of the smallest particle that produces a detectable pulse when it crosses the beam at the limit of the sensitive area. Between ϕ_2 and ϕ_1 the sensitive area decreases from S_T to 0, thus affecting the acceptance ratio R_{DOF}.

Figure 4 shows statistics of R_{DOF} (R_{EFF} for the Fast-FSSP) versus MVD, with scatterplots of 10-Hz samples, as well as the mean value and standard deviation, calculated every 1-μm step. In Fig. 4a, statistics are based on samples from the series of C-130 flights from hc9506 to hc9520 for the NCAR-FSSP (32 361 samples), and the complete series of Merlin-IV flights (me9505 to me9514) for the CAM probe (51 119 samples). Figure 4b for the Fast-FSSP is based on samples from two C-130 flights (hc9504 and hc9505) and the complete series of Merlin-IV flights (49 699 samples). The two figures exhibit the same feature with an increase of R_{DOF} and R_{EFF} with decreasing MVD values, which is in agreement with the laboratory measurements of Dye and Baumgardner (1984). Consequently, the CDNC values derived with a constant sampling section slightly overestimate the concentration of the small particles with respect to the large ones. Within the range from 10 to 20 μm, however, the Fast-FSSP R_{EFF} increases less than the FSSP-100 R_{DOF}.

Figure 5 shows the ratio of the Fast-FSSP R_{EFF} to the CAM-FSSP R_{DOF} values of Fig. 4, together with the ratio of their CDNC measured values, as functions of MVD. The CDNC underestimation of the Fast-FSSP with respect to the CAM-FSSP is noticeable in the range from 9 to 13 μm. At smaller droplet sizes the opposite is observed in agreement with the sharp increase of the Fast-FSSP R_{EFF} below 8 μm in Fig. 4b. This feature can be interpreted as a decrease of S_T below 8 μm which, combined with the increase of S_{EFF}, results in a sharp
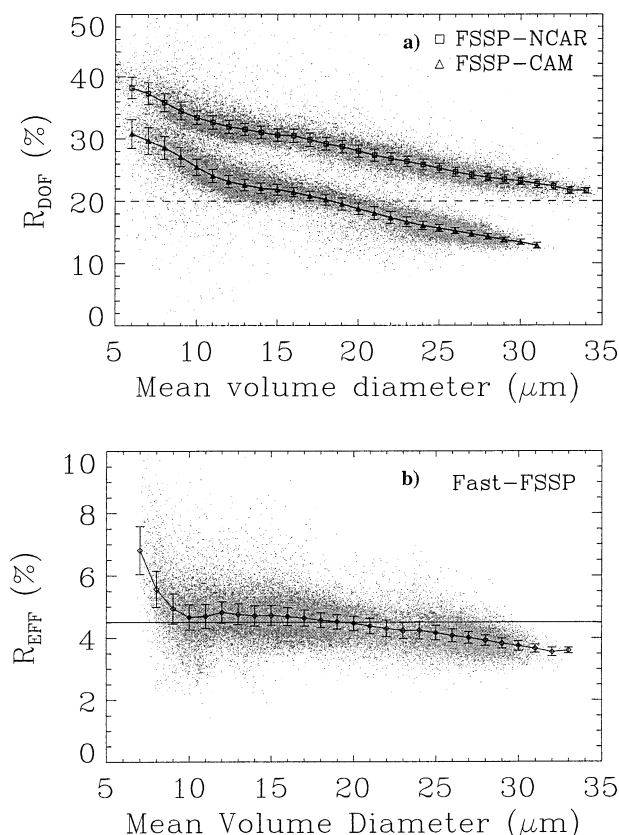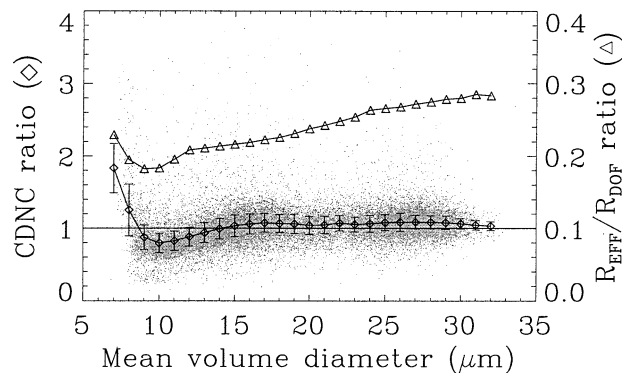
FIG. 5. Scatterplot of the 10-Hz sample ratio of the Fast-FSSP to CAM-FSSP CDNC measured values vs mean volume diameter (from the 10 Merlin-IV flights). Mean value (diamonds) and std dev are indicated for every 1-μm-diameter step. Mean values of the ratio of the Fast-FSSP R_{EFF} to the CAM-FSSP R_{DOF} values from Fig. 4 are added (triangles, right-hand scale).

FIG. 4. Scatterplot of the 10-Hz sample (a) R_{DOF} values vs mean volume diameter, as measured with the NCAR-FSSP (from NCAR C-130 flights hc9506 to hc9520) and the CAM-FSSP (from the 10 Merlin-IV flights), and (b) R_{EFF} values vs mean volume diameter measured with the Fast-FSSP (from NCAR C-130 flights hc9504 and hc9505, and the 10 Merlin-IV flights). Here R_{DOF} (R_{EFF}) is the ratio of DOF (*slit*) selected counts to the total counts. Mean value and std dev are indicated for every 1-μm-diameter step.

R_{EFF} increase at the lower limit of the probe's diameter range. This feature suggests that the threshold diameter ϕ_2 for a constant sensitive area is close to 8 μm.

In fact it is not feasible to directly derive S_{DOF} (S_{EFF} for the Fast-FSSP) from data collected in flight, only R_{DOF} (R_{EFF}) can be calculated. It is thus not feasible, from the comparison of Fast-FSSP versus CAM-FSSP, to determine firmly which one of the two probes is in error. This issue is addressed here by comparing both probe's estimations of LWC to the CSIRO measurements. Figure 6 shows the ratio of the FSSP-derived LWC, CAM-FSSP in Fig. 6a and Fast-FSSP in Fig. 6b, to the CSIRO measured one as a function of the FSSP-measured MVD, with mean value and standard deviation every 1-μm step in MVD. The data are the 10-Hz samples from the 10 Merlin-IV flights, with the condition that CDNC values are smaller than 300 cm^{-3} (35 105 samples) in order to avoid coincidence effects that are discussed in the next section. Assuming droplet sizing is accurate, the figure suggests that the CAM-FSSP overestimates the droplet concentration at MVD values smaller than 12 μm, while

the Fast-FSSP slightly underestimates the concentration at MVD values between 9 and 12 μm, and slightly overestimates the concentration at MVD values smaller than 9 μm. It must be noted though that the reliability of the CSIRO probe at small droplet sizes is also questionable (Biter et al. 1987).

These biases in the measurements of small droplet concentrations with FSSPs should not be considered as an incorrect setting of the probe optics or electronics, as it rather seems to be inherent to the optical principle. This feature is in fact well reproduced with the model of probe operation of Perrin et al. (1998). The difference between FSSP-100 and Fast-FSSP arises from the different sampling section selection techniques: *mask* for the FSSP-100 and *slit* for the Fast-FSSP. The slight difference between the CAM and the NCAR-FSSPs in Fig. 4a should be attributed to the different gain settings of the signal and annulus amplifiers, a feature that is also well reproduced with the model of probe operation. In summary, the variation of the efficient sampling section in both the FSSP-100 and the Fast-FSSP is a source of uncertainty that mainly affects the measurements of the small droplets, especially at sizes below 8 μm, where the sensitive area is also dependent on droplet size.

The pulse duration selection in the FSSP-100 is a second source of uncertainty in droplet spectra measurements. The procedure is based on the selection of detections with a pulse duration longer than the running mean. The Fast-FSSP that records the pulse duration for each detection is well suited for the examination of this selection procedure. In Fig. 7 the cumulative frequency distribution of pulse duration measured with the Fast-FSSP is reported for three narrow spectra sampled during the Merlin-IV flights me9507 and me9511. The left-hand side shows the cumulative distribution for all the detections (thin line), and for only the slit accepted ones (thick line). The dashed line illustrates the expected cumulative distribution for particles crossing a uniform
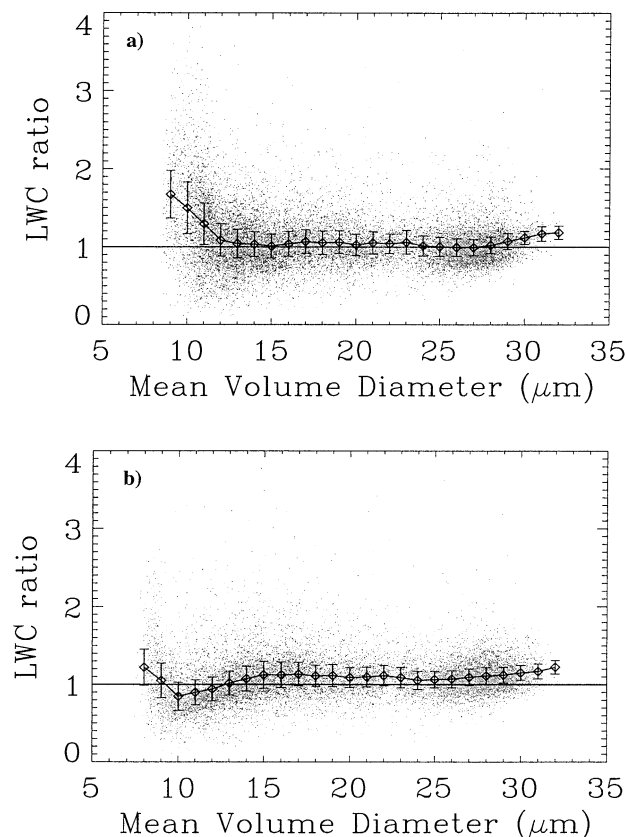
FIG. 6. Scatterplot of the 10-Hz sample ratio of LWC values derived from the droplet spectrum measured with (a) the CAM-FSSP and (b) the Fast-FSSP to the values measured with the CSIRO probe, as functions of mean volume diameter (same samples as in Fig. 5). Mean value and std dev are indicated for every 1-μm-diameter step.

cylindrical beam of 230-μm diameter. In order to avoid variations due to the aircraft speed, pulse durations are normalized to an aircraft speed of 100 m s^{-1}. The corresponding droplet spectrum for all the detections (thin line) and the slit-selected ones (thick line) is reported on the right-hand side. The values of mean droplet diameter in Figs. 7a,b,c are 8.4, 17, and 26 μm, respectively. The pulse duration distribution exhibits a tail toward long durations that is typical of the coincidence effects (Brenguier and Amodei 1989; Brenguier 1989). This issue will be discussed further. Note also the much sharper pulse duration distribution of the selected pulses that illustrates the efficiency of the slit technique for rejection of particles crossing the beam edge.

In the FSSP-100 the DOF selection procedure with the annulus only selects particles along the beam axis, that is, it includes particles crossing the beam edge. Their expected pulse duration statistics is thus represented by the dashed line in Fig. 7. Pulses with a duration longer than the mean correspond theoretically to particles crossing the beam within the 62% central section (Dye and Baumgardner 1984). When the droplet spectrum is narrow, this mean pulse duration selection

is efficient and FSSP-100 spectra compare well with the Fast-FSSP ones, as in Fig. 2. When the droplet spectrum is broad, however, the procedure is no longer reliable because the pulse duration also depends on the particle size. This is illustrated in Fig. 8 where Fast-FSSP measurements of pulse duration from flight me9511 are represented as a function of the droplet diameter. Pulse durations longer than 3 μs that are due to coincidences are not accounted for in the calculation of the mean. The thin line corresponds to all the detections and the thick line to the slit selected ones. Simplified models of the expected variation of pulse duration with particle diameter are also plotted. The dashed line represents the pulse duration of a Gaussian pulse with a variable amplitude, when sampled at a fixed detection threshold: $T = K\{2 \log[A(\phi)/A_0]\}^{1/2}$, where K is a constant, A_0 is the probe's detection threshold, and $A(\phi)$ is the pulse amplitude for a droplet of diameter ϕ. The dotted line represents the expected increase for particles entering a uniform beam: $T = (D + \phi)/v_a$, where D is the beam diameter and v_a is the aircraft speed.

This dependency is emphasized in Fig. 7 with the complete distribution of pulse duration that is slightly shifted depending on the mean droplet diameter. When the spectrum is broad, the resulting statistics of pulse duration can be regarded as a combination of such distributions, with an intermediate mean value. Consequently, some small droplets crossing within the 62% central region can be rejected, while large droplets crossing the beam outside of this central area can have a pulse duration longer than the mean and as such can be erroneously selected. Since they cross the beam in a region of reduced intensity, they are counted in a smaller size class than expected thus producing a significant spectrum broadening.

The consequence of this is illustrated in Fig. 9 that shows, as in Fig. 2, the comparison of spectra measured with the Fast-FSSP and the three FSSP-100s during the intercalibration flight. However, in Fig. 9 broad bimodal spectra are displayed that exhibit modes at 8 and 15 μm. The four examples are sorted by increasing proportions of the larger mode. In Fig. 9a, the four probes show the same narrow spectrum with a tail toward large particles. As the proportion of big droplets increases, from Fig. 9b to 9d, it is noticeable that the three standard probes measure a significant percentage of the big droplets in the intermediate size class between the two modes, and thus miss the bimodality of the spectra. The figure also reveals that the CAM-FSSP does not perform better than the two other FSSPs in the identification of bimodality, thus suggesting that the delay mode is not efficient at compensating this broadening effect.

c. Effects of coincidences

The coincidence of particles in the detection beam is a limitation inherent to any single particle counter. First of all, it is important to notice that only detections made

a) me9507 - 151435.3 (2500 ms) - 780 m

b) me9511 - 163454.1 (300 ms) - 940 m

c) me9511 - 152648 (1600 ms) - 2190 m

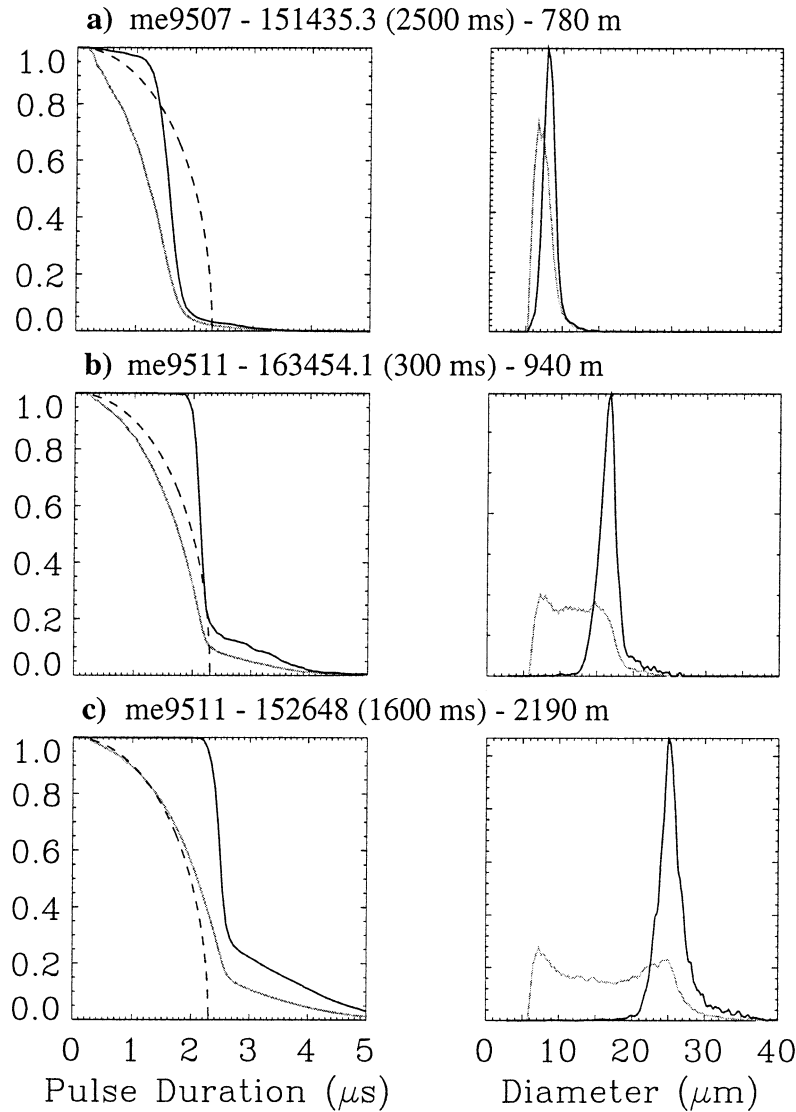Pulse Duration (μs)   Diameter (μm)

FIG. 7. Cumulative distributions of pulse duration measured with the Fast-FSSP for total counts (thin line) and the slit selected ones (thick line) on the left-hand side. The dashed line represents the statistics of particles crossing a uniform cylindrical beam of 230 μm in diameter. The corresponding spectra are represented on the right-hand side, based on total counts (thin line) and the slit selected ones (thick line). Flight number, sampling time (UTC), sample duration (ms), and sampling altitude (m), as indicated in the legend.

inside the efficient sampling section can be used for deriving a droplet spectrum (between 4% and 10% of the total), but that all the detections contribute to the probability of coincidence that is proportional to the sensitive volume of the instrument. The FSSP sensitive volume and efficient area are optimized for measurements of CDNC values up to 200 cm^{-3}. At higher concentrations coincidences affect droplet counting and sizing.

The Fast-FSSP is a pure retriggerable counter (no dead time) and the correction of the coincidence losses is trivial:

$$\lambda_a = \lambda_c/(1 - A), \qquad (2)$$

where λ_a is the actual droplet rate, λ_c is the counted rate, and A is the sum of the pulse durations per second, also referred to as the *Activity*. The indices i for the size class have been omitted, which means that it is assumed that all size classes are affected similarly by the coincidence losses. The accuracy of the Fast-FSSP correction is attested to by an alternative technique that is not sensitive to the coincidences, namely, the statistics of interarrival times between detections (Brenguier 1993; Burnet and Brenguier 1999).

The correction for the FSSP-100 is more complicated because of the probe dead time. It is applied to the CAM-
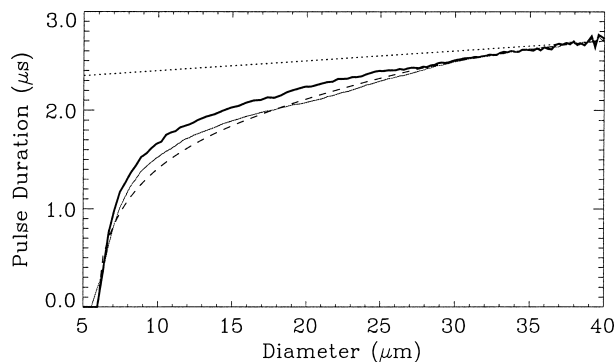
FIG. 8. Mean pulse duration from the Fast-FSSP measurements based on total counts (thin line) and slit selected counts (thick line) vs diameter. The expected increase of the pulse duration with droplet size, for a uniform beam, is indicated by the dotted line. The dashed line represents the expected pulse duration variation for a Gaussian pulse with a variable amplitude.

FSSP as indicated in Brenguier and Amodei (1989). For the NCAR-FSSP a simplified formula is used (Dye and Baumgardner 1984):

$$\lambda_a = \lambda_c/(1 - mA), \tag{3}$$

where A is now the sum of the pulse durations and dead times, and the coefficient m was empirically estimated to 0.55 for SCMS (NCAR-RAF processing). In fact, the theory shows that m is not a constant and that it tends to 1 when CDNC tends to infinity (Brenguier 1989).

Figure 10 shows the comparison of the 10-Hz CDNC-derived values after coincidence correction. In Fig. 10a, data are from the NCAR C-130 flight hc9505 (2542 samples). The Fast-FSSP is corrected using (2) and the NCAR-FSSP is corrected using (3). The NCAR-FSSP total counted rate to use in (3) (*total reset*) was not measured during flight hc9505. Therefore, it was initially derived from the DOF counted rate by assuming $R_{DOF} = 20\%$. However, the *total reset* was measured during the following flights and Fig. 4a shows that the actual R_{DOF} value is larger than 20% and that it depends on the droplet diameter. NCAR-FSSP data were thus reprocessed according to the best linear fit in Fig. 4a; that is, $R_{DOF} = 37.35-0.47$MVD. In Fig. 10b the data (1198 samples) are from the Merlin-IV flight me9514 and the Fast-FSSP is compared to the CAM-FSSP that is corrected with the technique of Brenguier (1989). Finally, Fig. 10c shows the same data as in Fig. 10b, with the CAM-FSSP data corrected using (3). As in the previous section, the first FSSP-100 class was not accounted for.

The Fast and the CAM-FSSP in Fig. 10b agree up to values as high as 800 cm^{-3}, while the NCAR-FSSP and the CAM-FSSP corrected with (3) show a saturation at about 500 cm^{-3}. Such a saturation of CDNC is not supported by the alternative technique based on inter-arrival time statistics, demonstrating that (3) underestimates the largest CDNC values. The values derived from the statistics of interarrival times in fact agree with
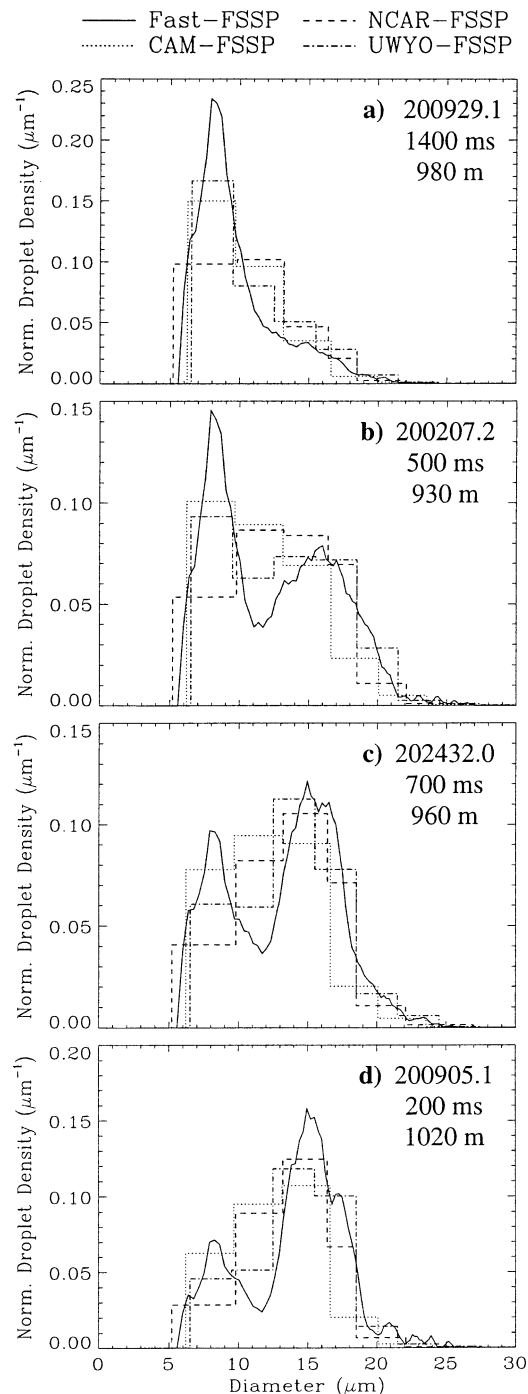

FIG. 9. Droplet spectra measured with the Fast-FSSP and the three FSSP-100s during the Merlin-IV intercalibration flight me9514. Sampling time (UTC), sample duration (ms), and sampling altitude (m), as indicated in the legend. The four spectra have been normalized to their respective total concentration for facilitating the comparison of the spectral shapes.

the values derived with (2) within 5%, up to values larger than 1000 cm^{-3} (Burnet and Brenguier 1999).

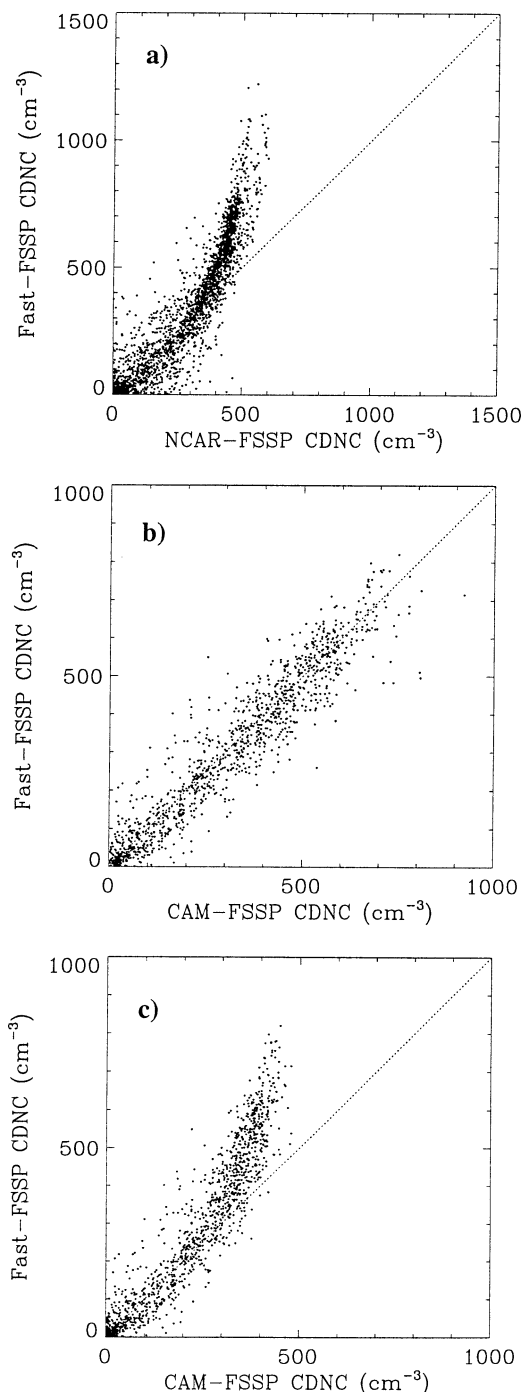Figure 11 shows the comparison of LWC values directly measured with the PVM-100A or the CSIRO

FIG. 10. Scatterplot of the 10-Hz CDNC values corrected for co-incidence losses, as measured with the Fast-FSSP vs (a) the values measured with the NCAR-FSSP (flight hc9505), (b) the CAM-FSSP corrected with the technique of Brenguier (1989) (flight me9514), and (c) the CAM-FSSP corrected by using (3) (flight me9514).

probe, with the values calculated by integration over the droplet spectra measured with the Fast-FSSP, corrected using (2), during flight hc9505 (2390 samples) in Fig. 11a; with the NCAR-FSSP, corrected using (3), during

the same flight (3134 samples) in Fig. 11b; and with the CAM-FSSP, corrected following Brenguier (1989), during the cloud traverses of flight me9508 with the highest CDNC values (422 samples) in Fig. 11c.

These comparisons of LWC are quite surprising and contradictory with the analysis of the CDNC measurements in the previous figure. The Fast- and the CAM-FSSP obviously overestimate LWC compared to either the PVM-100A in Fig. 11a for the Fast-FSSP or the CSIRO probe in Fig. 11c for the CAM-FSSP. This is attested by the calculated adiabatic LWC that provides a theoretical maximum value (for the data shown in Fig. 11c, e.g., sampled at about 600 m above cloud base, this upper limit is 1.4 g m^{-3}, while CAM-FSSP LWC measurements exceed 2 g m^{-3}). The NCAR-FSSP in Fig. 11b slightly underestimates LWC compared to the PVM-100A, but the discrepancy is small with regard to the sharp limitation of the CDNC measurements in Fig. 10a.

These features result from an additional effect of the coincidences; namely, the fact that a detection of co-incident droplets is statistically counted in a larger size class than the ones of those same droplets counted in-dividually (Perrin et al. 1998). The distortion is worse in the FSSP-100 because of the pulse duration selection procedure. The mean pulse duration is indeed length-ened by the longer pulses of coincident particles. This means that smaller droplets with short pulse durations can be biased out. The FSSP-100 droplet spectra are therefore shifted toward larger diameters than the Fast-FSSP ones at high coincidences rates. This effect is illustrated in Fig. 12 for four spectra measured at the same level, with increasing CDNC values. Table 4 sum-marizes characteristic values of the four spectra. The mean volume diameter measured with the Fast-FSSP is almost constant around 10.5 μm, with a spectrum width of about 2.15 μm. In contrast, the spectra measured with the CAM-FSSP exhibit MVD values increasing from 12.5 to 13.8 μm, with a spectral width increasing from 3.03 to 3.42 μm. Therefore, if only CDNC is corrected for coincidence losses, but the spectrum is not corrected for the shift toward larger diameters, the resulting LWC is overestimated. For the NCAR-FSSP corrected with (3), the underestimation of CDNC compensates the dis-tortion of the spectrum.

One can also notice in Table 4 that CDNC values measured with the Fast-FSSP only increase from 757 to 856 cm^{-3} over these four samples, while the CAM-FSSP CDNC values increase from 995 to 1458 cm^{-3}. This is in contrast with the general agreement between Fast-FSSP and CAM-FSSP CDNC values as illustrated in Fig. 10b. This additional discrepancy is due to var-iations of the Fast-FSSP efficient sampling section. Fig-ure 13 shows Fast-FSSP R_{EFF} values versus MVD in Fig. 13a, and versus the corrected CDNC value in Figs. 13b,c. The data are 10-Hz samples from the same Mer-lin-IV flight (me9508). The MVD graph shows two groups of samples, below and above 12 μm. The two
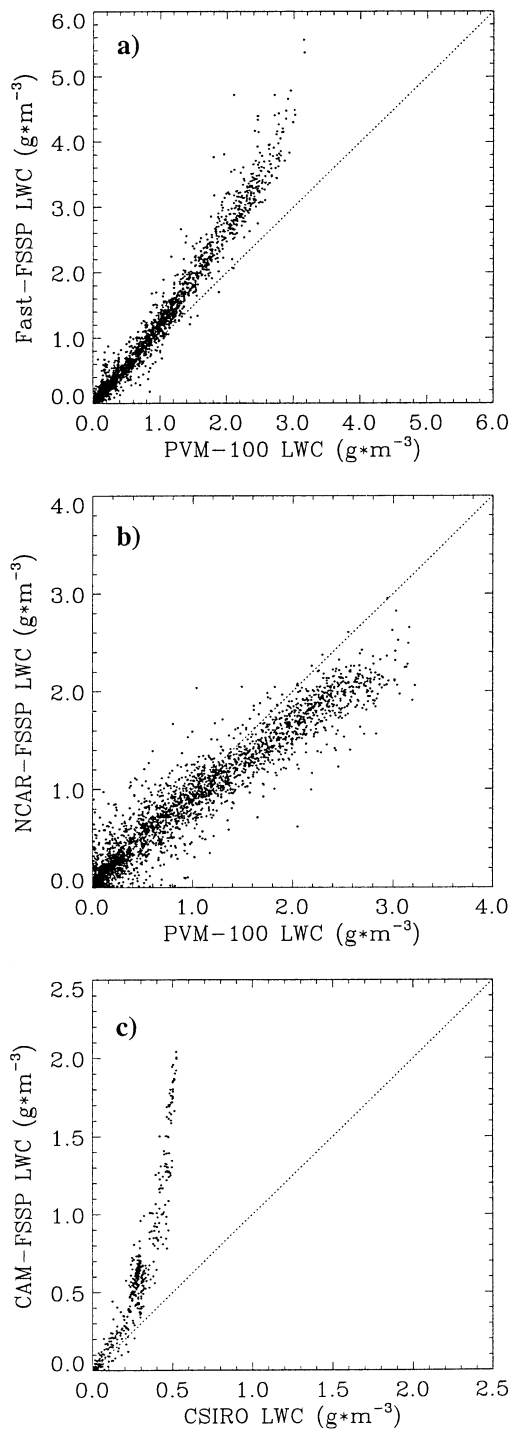
FIG. 11. Scatterplot of the LWC values derived from the FSSP droplet spectra vs PVM-100A and CSIRO measurements. (a) Fast-FSSP vs PVM-100A (flight hc9505), (b) NCAR-FSSP vs PVM-100A (flight hc9505), and (c) CAM-FSSP vs CSIRO (flight me9508, only cloud traverses with CDNC peak values greater than 800 cm^{-3}).

populations are plotted separately in Figs. 13b,c versus the CDNC value. Figure 13b reveals that R_{EFF} decreases with increasing CDNC values for samples with MVD smaller than 12 μm. The coincidences are thus reducing R_{EFF} when the droplets are small, hence leading to an underestimation of CDNC. It is likely that this feature is related to the probability for a coincidence of droplets to be selected, when some of the coincident droplets are crossing the beam outside of the efficient area, as discussed by Cooper (1988) for the standard FSSP.

The effects of the coincidence on the spectral shape and CDNC were demonstrated by Perrin et al. (1998) using the stochastic model of probe functioning that is, however, not usable for the retrieval of the actual spectrum from the measured one. Therefore, the FSSP (standard and Fast) spectra measured during SCMS are only corrected for the coincidence losses, but they are not corrected for spectral distortion. As mentioned above, the coincidence correction was applied similarly to all the size classes. Because of the spectral distortion and the variations of the efficient sampling section, the correction factor should in fact be size dependent. The stochastic model of probe functioning is presently used to better understand these features. They are presented here to show that under some circumstances FSSP measurements, either Fast or standard, can be significantly affected by the coincidences.

4. Summary of the Merlin-IV dataset

The microphysical dataset of the 10 Merlin-IV flights is summarized in Fig. 14, with the comparison of Fast-FSSP and CAM-FSSP measurements for CDNC and the CSIRO probe for LWC. The dataset consists of 10-Hz samples from 350 samples during the shortest flight (me9513) up to 7500 samples during the longest one (me9505). For each comparison, the ratio of the 10-Hz measured values is calculated, and its statistics is represented in Fig. 14 by the mean ratio (black dots) and the 20% and 80% percentiles of its cumulative frequency distribution (vertical bars). In addition, each flight is also characterized by the mean and the maximum values of the considered parameter, as measured by the Fast-FSSP. The maximum value is defined as the 98% percentile of the cumulative frequency distribution of the parameter.

The Fast- and the CAM-FSSPs show a very good agreement for the measurements of CDNC with a bias lower than 10% and a dispersion of ±20%, as expected with these instruments (Brenguier et al. 1994). The LWC-derived values show more discrepancy because LWC calculations accumulate errors on CDNC and errors on droplet sizes. In particular, it must be noted that the Fast-FSSP experienced a progressive loss of sensitivity during the campaign that was accounted for by the self-calibration technique (Brenguier et al. 1998). Such a procedure is not applicable to the FSSP-100 because it requires the very fine size resolution of the
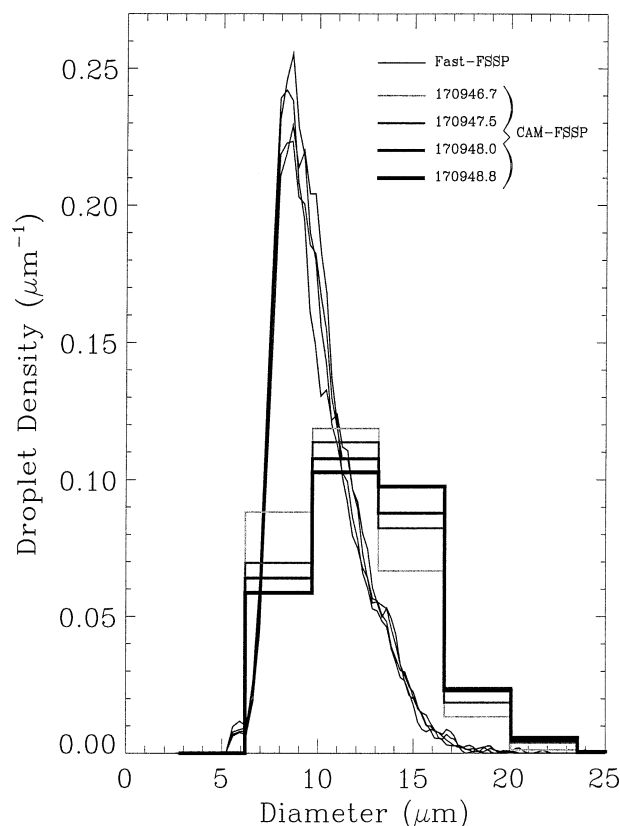
FIG. 12. Droplet spectra measured with the Fast-FSSP and the CAM-FSSP during the Merlin-IV flight me9508. The four spectra are from the cloud traverse 1709:46–1709:57 UTC at an altitude of 1200 m (about 700 m above cloud base). Each spectrum is an average over 300 ms at sampling time (UTC) as indicated in the legend. The four CAM-FSSP spectra are plotted with gray level and line thickness increasing with increasing CDNC values. As in Fig. 9, the spectra have been normalized to their respective total concentration.

TABLE 4. Characteristics of the four droplet spectra shown in Fig. 12.

Sampling time (UTC)	Fast-FSSP	CAM-FSSP
1709:46.7		
CDNC (cm^{-3})	757	995
Mean vol diam (μm)	10.58	12.52
Spectral width (μm)	2.14	3.03
1709:47.5		
CDNC (cm^{-3})	801	1167
Mean vol diam (μm)	10.42	13.21
Spectral width (μm)	2.07	3.23
1709:48.0		
CDNC (cm^{-3})	851	1381
Mean vol diam (μm)	10.63	13.52
Spectral width (μm)	2.19	3.34
1709:48.8		
CDNC (cm^{-3})	856	1458
Mean vol diam (μm)	10.57	13.80
Spectral width (μm)	2.19	3.42

sea salt, it is likely that the FSSP-100 was also affected and that it progressively underestimated the droplet sizes. This is reflected in the comparison by the positive LWC bias increasing with time (up to 30% on flight me9514).

This hypothesis is corroborated by the CSIRO probe. Its comparison with the Fast-FSSP-derived LWC shows no trend (Fig. 14d), while the comparison with the CAM-FSSP-derived LWC shows a progressive underestimation by the CAM-FSSP (Fig. 14e). Overall, the Fast-FSSP slightly overestimates LWC with respect to the CSIRO probe. On me9509 the ratio of Fast-FSSP to CSIRO LWC, however, increases up to 70%. This is due to the high CDNC values encountered during this flight that are responsible for a significant distortion of the measured spectra toward larger sizes than expected, hence resulting in the overestimation of LWC by the Fast-FSSP, while the CSIRO probe is not affected by the coincidences. Except for the coincidence effects, LWC measurements stay within an uncertainty range of
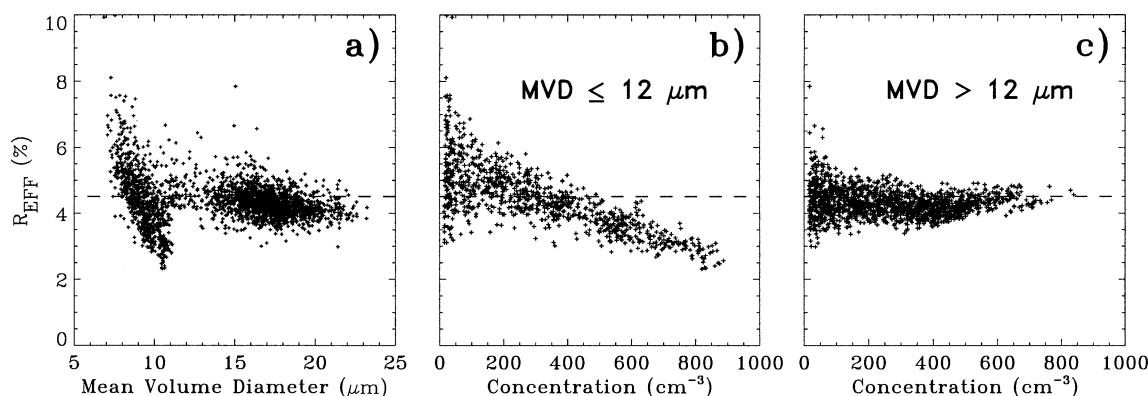
Fast-FSSP. Consequently, the size calibration of the FSSP-100 was kept constant over the whole campaign duration. Since the sensitivity loss of the Fast-FSSP was probably due to contamination of the optics by dust and

FIG. 13. Scatterplot of the R_{EFF} 10-Hz sample values measured with the Fast-FSSP during the Merlin-IV flight me9508, vs (a) MVD and (b),(c) CDNC for samples with MVD values smaller and greater than 12 μm, respectively.
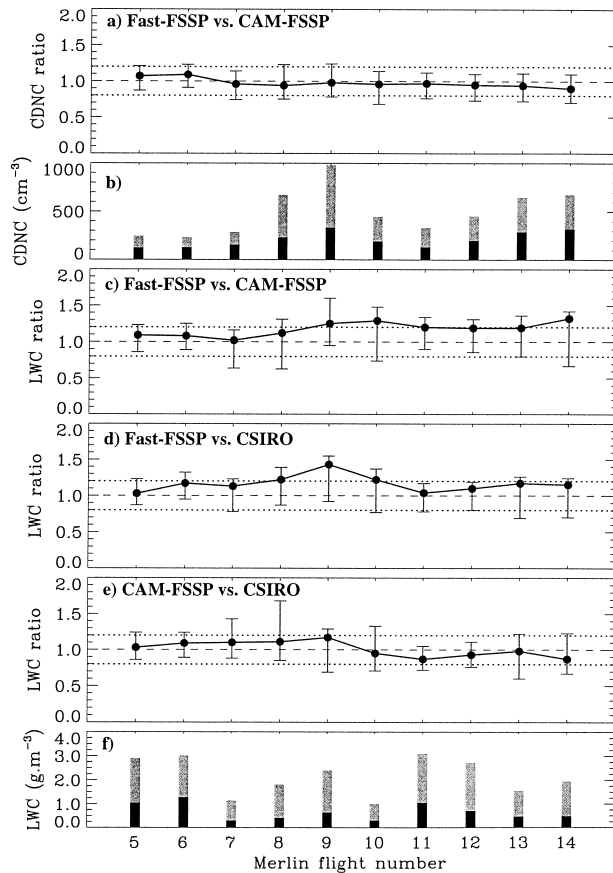
FIG. 14. Summary of the Merlin-IV dataset. Flight-by-flight comparison between instruments with statistics of the ratio of the 10-Hz measured values: (a) Fast-FSSP vs CAM-FSSP CDNC, (c) Fast-FSSP vs CAM-FSSP LWC, (d) Fast-FSSP vs CSIRO LWC, (e) CAM-FSSP vs CSIRO LWC. Each flight is characterized by the mean value (black dot), the 20% and the 80% percentiles (vertical bars) of the frequency distribution of the ratio of both measurements. (b), (f) The mean (black) and maximum (gray) values of CDNC and LWC, respectively, as measured with the Fast-FSSP.

$\pm 30\%$, which is remarkable considering the differences between the two probe's operations.

5. Conclusions

The analysis of the large SCMS dataset, combining FSSP-100, Fast-FSSP, CSIRO, and PVM-100A measurements, provides high statistical significance in the characterization of the FSSP limitations. The conclusions are briefly summarized here.

- *Size calibration:* The standard linear calibration of the FSSP-100 introduces a bias in the measurements of the small droplet sizes, overestimation of the diameter below 11 μm, and underestimation of the diameter in the range from 12 to 18 μm. Otherwise, the data from various FSSP-100 instruments agree within a standard deviation of ± 1 μm in mean volume diameter, over the whole diameter range.

- *Beam inhomogeneities:* The FSSP-100, with a sampling section for sizing of 0.3 mm² (10% selection ratio), shows more spectrum broadening due to beam inhomogeneities than the Fast-FSSP, which has a smaller *efficient* sampling section of 0.13 mm² (4.5% selection ratio). This results in a 0.5-μm overestimation of the spectral width by the FSSP-100 with respect to the Fast-FSSP. The sampling section can be electronically adjusted and reduced to an area of more uniform laser intensity, but it must be noted that a small sampling section also implies a reduced sampling rate, hence a poor statistical significance of the measured samples.

- *Variations of the sampling section:* The DOF sampling section of the FSSP probes, both standard and Fast, increases with decreasing droplet size. It is not feasible to precisely document the dependence of S_{DOF} with the droplet diameter from data collected in flight because the measured spectra are not monodispersed (MVD is used here as an indication of the mean droplet size) and because S_{DOF} is not directly measurable; only $R_{DOF} = S_{DOF}/S_T$ can be recorded. The analysis of the Fast-FSSP dataset suggests that S_T is constant down to about 8 μm in droplet diameter and that it decreases substantially for smaller droplets. In contrast S_{DOF} increases continuously with decreasing droplet sizes. These variations are probe dependent and can be significant (e.g., the increase of the FSSP-CAM S_{DOF} from 31 to 8 μm exceeds a factor of 2). Consequently, the concentration density of the small droplets is overestimated with respect to the density of the big ones.

- *Pulse duration selection:* The procedure is efficient at rejecting particles crossing the beam edge when the spectrum is narrow and CDNC is low. The dependence between pulse duration and droplet size, however, introduces a bias when the spectrum is broad. The largest droplets are preferentially selected with respect to the smallest ones, but they are counted in a smaller size class than ideal. This can prevent the detection of bimodal spectra. This effect is accentuated at high CDNC values by the coincidence of particles that lengthen the mean pulse duration. The *pulse duration* selection procedure is not used in the Fast-FSSP, which is thus not affected by this limitation.

- *Coincidences:* Coincidences of particles in the beam lead to an underestimation of the droplet concentration. That can be accurately compensated by using the statistical correction procedure of Brenguier (1989). Coincidences also produce a distortion of the droplet spectrum toward larger sizes than ideal, which introduces a significant overestimation of the derived LWC. Finally, coincidences can be responsible for variations of the *efficient* sampling section, depending on the droplet size. It has been shown, for example, that under specific conditions (high CDNC of small droplets), Fast-FSSP measurements of CDNC can be noticeably underestimated.

The size calibration bias, the broadening by beam inhomogeneities, and the coincidence losses can be corrected using straightforward procedures, such as the transfer matrix proposed by Cooper (1988), which linearly relates the measured spectrum to the actual one. However, spectra distortion due to variations of the sampling section, especially the one related to the *pulse duration* selection and to the coincidence of particles, cannot be linearized. In fact, the transfer matrix depends upon the actual droplet spectrum. Therefore, no operational procedure exists for correction of these effects. They can be precisely simulated with the stochastic model of probe functioning of Perrin et al. (1998), but, as in any stochastic (nondeterministic) model, it is more difficult to invert than the Cooper (1988) matrix model for the retrieval of actual spectra from the measured ones. Alternative approaches are presently tested.

Except for the above-mentioned limitations, the SCMS dataset collected with the Merlin-IV instrumented aircraft is consistent in terms of droplet concentration and liquid water content. A complete catalogue of the analysis is available upon request to the lead author.

REFERENCES

Baumgardner, D., 1986: A new technique for the study of cloud microstructure. *J. Atmos. Oceanic Technol.,* **3,** 340–343.
——, and M. Spowart, 1990: Evaluation of the Forward Scattering Spectrometer Probe. Part III: Time response and laser inhomogeneity limitations. *J. Atmos. Oceanic Technol.,* **7,** 666–672.
——, W. J. Strapp, and J. E. Dye, 1985: Evaluation of the Forward Scattering Spectrometer Probe. Part II: Corrections for coincidence and dead-time losses. *J. Atmos. Oceanic Technol.,* **2,** 626–632.
——, J. E. Dye, B. W. Gandrud, and R. G. Knollenberg, 1992: Interpretation of measurements made by the Forward Scattering Spectrometer Probe (FSSP-300) during the airborne Arctic stratospheric expedition. *J. Geophys. Res.,* **97,** 8035–8046.
Biter, C. J., J. E. Dye, D. Huffman, and W. D. King, 1987: The drop-size response of the CSIRO liquid water probe. *J. Atmos. Oceanic Technol.,* **4,** 359–367.
Bower, K. N., and T. W. Choularton, 1988: The effects of entrainment on the growth of droplets in continental cumulus clouds. *Quart. J. Roy. Meteor. Soc.,* **114,** 1411–1434.
Brenguier, J.-L., 1989: Coincidence and dead-time corrections for particle counters. Part II: High concentration measurements with an FSSP. *J. Atmos. Oceanic Technol.,* **6,** 585–598.
——, 1993: Observations of cloud microstructure at the centimeter scale. *J. Appl. Meteor.,* **32,** 783–793.
——, and L. Amodei, 1989: Coincidence and dead-time corrections for particle counters. Part I: A general mathematical formalism. *J. Atmos. Oceanic Technol.,* **6,** 575–584.
——, and L. Chaumat, 2001: Droplet spectra broadening in cumulus clouds. Part I: Broadening in adiabatic cores. *J. Atmos. Sci.,* **58,** 628–641.
——, D. Baumgardner, and B. Baker, 1994: A review and discussion of processing algorithms for FSSP concentration measurements. *J. Atmos. Oceanic Technol.,* **11,** 1409–1414.
——, T. Bourrianne, A. Coelho, J. Isbert, R. Peytavi, D. Trevarin, and P. Weschler, 1998: Improvements of droplet size distribution measurements with the Fast-FSSP (Forward Scattering Spectrometer Probe). *J. Atmos. Oceanic Technol.,* **15,** 1077–1090.
Burnet, F., and J.-L. Brenguier, 1999: Validation of droplet spectra and liquid water content measurements. *Phys. Chem. Earth,* **24B,** 249–254.
Chaumat, L., and J.-L. Brenguier, 2001: Droplet spectra broadening in cumulus clouds. Part II: Microscale droplet concentration heterogeneities. *J. Atmos. Sci.,* **58,** 642–654.
Cooper, W. A., 1988: Effects of coincidence on measurements with a Forward Scattering Spectrometer Probe. *J. Atmos. Oceanic Technol.,* **5,** 823–832.
Dye, J. E., and D. Baumgardner, 1984: Evaluation of the Forward Scattering Spectrometer Probe. Part I: Electronic and optical studies. *J. Atmos. Oceanic Technol.,* **1,** 329–344.
Gerber, H., B. G. Arends, and A. S. Ackerman, 1994: New microphysics sensor for aircraft use. *Atmos. Res.,* **31,** 235–252.
Hill, T. A., and T. W. Choularton, 1985: An airborne study of the microphysical structure of cumulus clouds. *Quart. J. Roy. Meteor. Soc.,* **111,** 517–544.
King, W. D., D. A. Parkin, and R. J. Handsworth, 1978: A hot-wire liquid water device having fully calculable response characteristics. *J. Appl. Meteor.,* **17,** 1809–1813.
Lawson, R. P., and R. H. Cormack, 1995: Theoretical design and preliminary tests of two new particle spectrometers for cloud microphysics research. *Atmos. Res.,* **35,** 315–348.
Norment, H. G., 1988: Three-dimensional trajectory analysis of two drop sizing instruments: PMS OAP and PMS FSSP. *J. Atmos. Oceanic Technol.,* **5,** 743–756.
Perrin, T., J.-L. Brenguier, and T. Bourrianne, 1998: Modeling coincidence effects in the Fast-FSSP with a Monte-Carlo model. Preprints, *Conf. on Cloud Physics,* Everett, WA, Amer. Meteor. Soc., 112–115.
Wendisch, M., A. Keil, and A. V. Korolev, 1996: FSSP characterization with monodisperse water droplets. *J. Atmos. Oceanic Technol.,* **13,** 1152–1165.